Supersonic and Transonic Adjoint-based Optimization of Airfoils

João P. Lourenço

joaoplourenco@tecnico.ulisboa.pt

Instituto Superior Técnico, Universidade de Lisboa, Portugal

November 2018

A robust and efficient high-fidelity aerodynamic shape optimization (ASO) methodology for airfoil shape optimization resorting to open-source platforms for computational fluid dynamics simulations was developed. This framework integrates open source codes: SALOME for the mesh generation; SU2 software for the aerodynamic shape optimization; and ParaView for post-processing. Two geometry parametrization methods, Hicks-Henne and Free-Form Deformation (FFD) methods are considered. All optimizations were performed using the adjoint method to compute sensitivities. The first case-study is a benchmark case which consists in drag minimization of the RAE 2822 airfoil in transonic viscous flow subject to lift, pitching moment and area constraints. Similar results to those found in the literature in terms of drag coefficient and computational cost were obtained showing the capability of the implemented ASO framework. In the second case-study, the aim was to maximize the lift to drag ratio starting with a NACA 0012 airfoil at zero degrees of angle of attack in inviscid conditions for two flow regimes (transonic and supersonic). For the FFD method a suitable definition of the box was set and the number of control points was allowed to change, while for the Hicks-Henne method both width bump control parameter and number of bump functions were analyzed. Regarding the number of design variables, the same behavior was found: increase of the lift to drag ratio and computational cost. In overall, they were able to increase pressure difference to increase lift which combined with an area reduction resulted in lift to drag ratio increase.

1. Introduction

Technological advances, and consequently the growth of the aeronautical sector, have led several companies to invest in commercial software or in creating their own codes. Not all companies, such as small and medium-size enterprises (SMEs), have the opportunity of obtaining commercial software given their excessive cost and developing their own code takes time, validation and resources. In the current days, high-fidelity Aerodynamic Shape Optimization (ASO) framework usually recur to commercial software or software developed by the companies themselves. Therefore, a robust and efficient high-fidelity ASO methodology using the adjoint method that employs only open source tools is developed.

A high fidelity ASO can result in high computational costs when traditional methods are applied to compute the gradients, such as the finite difference method which is used in most of gradient-based optimizers for sensitivity analysis [1]. The adjoint method have brought the possibility to improve the computational efficiency of ASO, when dealing with several design variables since it computes the gradients with greater accuracy and efficiency, thus reducing computational costs [2]–[4]. Over the last decades, shape optimization with adjoint method has been successfully applied to 2-D [5], [6] and 3-D configurations [7]–[9]. Jameson [2] was one of the first to propose an ASO based on systems governed by partial differential equations (PDEs). The adjoint method was extended together with the inviscid Euler equations in compressible flows and it was revealed to be appropriate for the design of transonic airfoils. The methodology was extended to performed an ASO of complex aircraft configurations [10]. In Anderson and Venkatakrishnan [11], the adjoint method for obtaining sensitivity derivatives and boundary conditions were derived for the incompressible Navier-Stokes (N-S) equations without the inclusion of turbulence effects. This inclusion was performed by Elliot *et al.* [12], along with the discrete adjoint implementation for the compressible N-S equations. Jameson *et al.*[13] presented the adjoint method for optimal aerodynamic design considering flows governed by the compressible N-S equations, which was successfully applied to the design of a wing in transonic flow. Anderson and Bonhaus [5] performed a 2-D design optimization methodology using the discrete adjoint approach and including the Spalart-Allmaras (SA) turbulence model for viscous flows. Nielsen and Anderson [8] achieved a drag reduction for the ONERA M6 wing using a 3-D Reynolds-Averaged Navier-Stokes (RANS) equations coupled with a SA turbulence model.

The goal main of this research is the development of a high fidelity computational framework to perform an aerodynamic shape optimization of an airfoil using Computational Fluid Dynamics (CFD), where one can use different

parameterization techniques, turbulence models, meshes and optimization settings resourcing to python scripts and open-source software for pre and post-processing. In addition, the impact of the parameterization methods on the airfoil shape will be analyzed. The optimization framework methodology will be applied to a first case of study to achieve the drag minimization of the RAE 2822 airfoil in transonic viscous flow, which a benchmark problem defined by the AIAA Aerodynamic Design Optimization Discussion Group (ADODG). In the second case, the aim is to maximize the lift to drag ratio for two Mach regimes (transonic and supersonic), starting from a NACA 0012 airfoil.

2. Theoretical background

To contextualize the theory applied to the following work, a brief introduction to the governing equations, optimization with gradients computed with the adjoint method, and the parameterizations methods is presented.

A. Governing equations of fluid dynamics and boundaries conditions

The equations governing the motion of a fluid and the evolution of its properties are differential equations, derived from the conservation laws such as mass, momentum and energy. The CFD module implemented in SU^2 is able to solve different physical models. The compressible Euler and RANS equations on a domain $\Omega \subset R^3$ are used to describe the viscous and inviscid flow around the aerodynamic shapes [14]. The conservation RANS equations can be described in differential form as [15]:

$$\frac{\partial(\mathbf{U})}{\partial t} + \nabla \cdot \mathbf{F}^C - \nabla \cdot \mathbf{F}^\upsilon - \mathbf{S}_\emptyset = \mathfrak{R}(\mathbf{U}) = 0 \text{ in } \Omega, t > 0. \quad (2.1)$$

where $\mathbf{U}$ represents the vector of state variables, $\mathbf{F}^C(\mathrm{U})$ and $\mathbf{F}^\upsilon(\mathrm{U})$ are the convective and viscous fluxes, respectively, $\mathbf{S}_\emptyset(\mathrm{U})$ is the source term and $\mathfrak{R}(\mathbf{U})$ is the numerical residual for the equations. By neglecting the terms $\mathbf{S}_\emptyset(\mathrm{U})$ and $\mathbf{F}^\upsilon(\mathrm{U})$, the Euler equations are achieved. The governing equation are numerically solved using a finite volume method (FVM) on a vertex-based median-dual grid. The classical Jameson–Schmidt–Turkel (JST) scheme is used to discretize the equations in space and the solution is marched forward in time using the implicit Euler scheme until a steady state is achieved. To deal with the viscous terms, the one-equation SA turbulence model is used. The compressible RANS solver in SU^2 supports several boundary condition types [16]. The list of available boundaries conditions makes the SU^2 a suitable solver for external and internal flows. It is considered the equations in a domain with a disconnected boundary divided in far-field, Γ_∞, and a solid wall representing the airfoil surface, S. A no-slip boundary condition is enforced at the airfoil surface together with an adiabatic condition. In the cases of inviscid flows, there is no friction to promote its sticking to the surface. This means that the flow velocity vector, $\boldsymbol{u}$, immediately adjacent to the wall must be tangent to the wall. Therefore, the non-penetrability condition is used. In the far-field, a characteristic-based boundary condition is applied, with $\mathbf{C}$ representing the characteristic variables [17]. The boundary conditions applied to the domain and the airfoil surface for a viscid flow can be described as:

$$\boldsymbol{u} = 0 \text{ on } S, \quad (2.2)$$

$$\left(\frac{\partial T}{\partial n_s}\right) = 0 \text{ on } S, \quad (2.3)$$

$$(\mathbf{C})_+ = \mathbf{C}_\infty \text{ on } \Gamma_\infty. \quad (2.4)$$

B. Adjoint solver and gradient evaluation

One of the key features of SU^2 is its capability to perform optimal shape design based on the discrete and continuous adjoint approach. Only the discrete adjoint approach is used to solve the adjoint Euler and RANS equations. In gradient-based optimization, the optimizer needs to establish a new search direction and, for this propose, it is necessary for the gradient to be evaluated in each design step. SU^2 uses the adjoint formulation to compute the sensitives of the objectives and constraint functions. Therefore, the functions gradients are computed through the chain rule by relating the geometric and surface sensitivities, which provides flexibility for the use of other parameterization methods [18], [19]. The sensitivity of the function of interest with respect to the design variables, is given by:

$$\begin{bmatrix} \frac{\partial I}{\partial D_1} \\ \vdots \\ \frac{\partial I}{\partial D_{n_D}} \end{bmatrix} = \begin{bmatrix} \frac{\partial s_1}{\partial D_1} & \cdots & \frac{\partial s_\sigma}{\partial D_1} \\ \vdots & \ddots & \vdots \\ \frac{\partial s_1}{\partial D_{n_D}} & \cdots & \frac{\partial s_\sigma}{\partial D_{n_D}} \end{bmatrix} \begin{bmatrix} \frac{\partial I}{\partial s_1} \\ \vdots \\ \frac{\partial I}{\partial s_\sigma} \end{bmatrix} \tag{2.5}$$

where σ is the number of surface mesh nodes and s_i $(i = 1, \dots, \sigma)$ are the local surface normal displacement for each discrete mesh node on the geometry surface. The term $\partial \boldsymbol{I}/\partial s$, surface sensitivities, represents the variation of the function of interest with respect to infinitesimal perturbations of the geometry shape in local surface normal direction. The geometric sensitivities, given by the Jacobian $\partial s/\partial \boldsymbol{D}$, measure the influence that the change of design variables has on the position of each grid point on the surface mesh.

C. Optimization framework

Aerodynamic properties are used to analyze the performance of an airfoil and, when a shape optimization is carried out, they can be mathematically seen as objective or constraint functions to the design. ASO problem involves the minimization of a chosen objective function, with respect to changes in the boundary shape, through the manipulation of a set of design variables. The design variables can be mathematically defined to parameterize the shape of an airfoil through a given parametrization method (presented latter in this work). Within a gradient-based optimization method, the gradients are used to guide the design towards an optimum design. For each new step, a new set of design variables is produced, causing a change in the objective function. A general constrained optimization problem can be defined according to:

$$\begin{aligned} \text{minimize} \quad & f(\mathbf{D}) \\ \text{w.r.t} \quad & \mathbf{D}, \\ \text{subject to} \quad & g_{\mathrm{j}}(\mathbf{D}) \leq 0, \ \mathrm{j} \in \{1, \dots, \mathrm{m}\} \\ & h_{\mathrm{k}}(\mathbf{D}) = 0, \ \mathrm{k} \in \{1, \dots, l\} \end{aligned} \tag{2.6}$$

where $\mathbf{D}$ is the vector of n_D design variables, f is the objective function to be minimized, or maximized, g_{j} and h_{k} are sets of inequality and equality constraint functions, respectively, to be satisfied. For the present work, the Sequential Least SQuare Programming (SLSQP) optimization algorithm is used. The convergence of the optimization process is achieved when the Karush-Kuhn-Tucker (KKT) optimality condition is within the tolerance imposed (10^{-10} by default). However, if this parameter is not satisfied the optimization process will stop when the maximum number of iterations is exceeded (100 by default).

D. Geometry Parameterization Methods

Shape parameterization has acquired a significant role in airfoil design and optimization. The success of optimization process is dependent on the parametric description of the object geometry which influences the computational time cost of the optimization as well as the quality of its results. Two parameterization methods embedded in SU^2 code are applied in this study, the Hicks-Henne bump functions [20] and the free-form deformation (FFD) method [21]–[23].

i. Free-Form Deformation

In the 80's, Sederberg and Parry [21] presented a classic technique for deforming solid geometric models in a free-form manner, that can deform surfaces of any type or degree such as planes or conic sections. The idea of FFD parameterization is to embed a flexible object into a parallelepiped lattice of control points that define the parametric space. By modifying the lattice, a deformation is transmitted to the included object in a similar way, creating a new shape. The FFD control volume (or FFD box) has a topology of a parallelepiped form when deforming 3-D objects or a rectangular plane for 2-D, so that it can be parameterized. Depending on the desired deformation, with FFD is possible to deform part of the domain while keeping the rest undeformed. The mathematical formulation of the classic FFD method is fully described for 3-D cases in [21]. Here, it is only presented the 2-D formulation (which was applied to the cases of study) that is discussed in detail in [24]. The Bézier surface FFD technique deforms a 2-D shape by embedding

it with a Bézier surface constrained to a plane which is controlled by the associated control points. The initial airfoil deformation $X^{initial} = (x^{initial}, y^{initial})$ with respect to a set of $n \times l$ Bézier surface control points $\mathbf{P}_{ij}$ is given by:

$$X = \sum_{j=0}^{l} \sum_{i=0}^{n} B_i^n \left(\frac{x^{initial} - x_{min}}{x_{max} - x_{min}} \right) B_j^l \left(\frac{y^{initial} - y_{min}}{y_{max} - y_{min}} \right) \mathbf{P}_{ij}, \quad \textbf{(2.7)}$$

where B_i^n and B_j^l are the Bernstein polynomials of degree n and l, respectively. Note that (x_{min}, y_{min}) and (x_{max}, y_{max}) are the corners of a deformation region. The number of control points is given by $n+1$ vertical columns and $l+1$ horizontal rows. The control points of the FFD box are defined as design variables, a number which depends on the degree of the chosen Bernstein polynomials. $\mathbf{P}_{ij}$ are the homogeneous coordinates of the displaced control point i, j defined by $\mathbf{P}_{ij} = \omega_{ij}(x_{ij}, y_{ij}, 1)$, where ω_{ij} is the weight parameter. Being all the weight $\omega_{ij} = 1$ and the lattice of control points rectangular, the initial control point positions are given by:

$$\mathbf{P}_{ij}^{initial} = \left(x_{min} + \frac{i}{n}(x_{max} - x_{min}), y_{min} + \frac{j}{l}(y_{max} - y_{min}) \right). \quad \textbf{(2.8)}$$

Due to its multiple advantages, the method is widely used in ASO of 2-D [25], [26] and 3-D [27] configurations, allowing to deform shapes with a minimal set of design variables. The FFD parameterization method has several powerful advantages being one of them the ability to deform almost any type of geometrical model. This ability is due to its formulation being independent of the object's mesh topology. The FFD technique can control surface continuity as well as volume preservation [28]. Regarding the SU² code, the method is numerically executed in three steps. Firstly, to embed the object, a mapping is performed from the physical domain to the parametric domain of the FFD box. This is performed only once before the optimization. The parametric coordinates of each node of the surface mesh are determined and persist unchanged during the design optimization cycle. In the second step, the structure of FFD control points is perturbed, deforming the FFD box together with the embedded object. Finally, when the FFD box has been deformed, the new Cartesian coordinates of the object in the physical domain are computed and a new shape can be study. The influence of one control point in the initial airfoil geometry is presented in Figure 1(a). The thickness at specific chordwise position of the airfoil can be modified by manipulating the control points.

ii. Hicks-Henne bump functions

In 1978, Hicks and Henne introduced an analytical approach to parameterize aerodynamic profiles [20]. Their compact formulation consists in using a base airfoil to which is added a linear combination of shape (or "bump") functions to perturb the upper and lower surface of the initial geometry. The new airfoil shape can be written according to the function:

$$y = y_{baseline} + \sum_{i=1}^{m} \Theta_i f_i(x), \; 0 \le x \le 1 \text{ with } f_i(x) = \left[\sin\left(\pi x^{\frac{\ln(0.5)}{\ln(h_i)}} \right) \right]^{t_i}, \quad \textbf{(2.9)}$$

where m is the number of bump functions; the coefficients Θ_i for $i = 1, \ldots, m$, employed to control the magnitude of the shape functions and acts as the weighting coefficients, are the design variables; $f_i(x)$ are the Hicks-Henne bump functions; h_i is the location of the maximum point of the bump function and t_i controls the width of the bump. The contribution of each parameter is determined by the value of the coefficients Θ_i associated to that function. If all the coefficients Θ_i are set to zero, the first computation gives the baseline geometry. Using this weighted sum of Hicks-Henne sine "bump" functions it is possible to achieve the desirable parameterized geometry [29]. The baseline airfoil shape, $y_{baseline}$, is deformed to yield a new airfoil shape, y. Each bump function, $f_i(x)$, is defined by three variables, each of which can be optimized or fixed [30], [31]. To ensure that the optimization process is only a function of the design variables, Θ_i, the bump width control parameter t and the bump maximum positions h_i are kept fix during the optimization. For the bump width control parameter t_i, a default value of 3 is set in the SU² code. In the present work, the default value of 3 is used for the first case, while a range of values from 2 to 10 is set for the second case to analysis the impact on the optimization design. For the bump maximum positions h_i, an equally-distributed over the range $[0.05/m, 1 - 0.5/m]$ is selected. Figure 1(b)**Erro! A origem da referência não foi encontrada.** illustrates the distribution

of the bump maximum positions for 15 bump functions along the NACA 0012 airfoil. Same set of distribution is used for the RAE 2822 airfoil. The Hicks-Henne functions can be chosen according to the region that we want to refine by keeping the remaining object to be optimized virtually undisturbed. One disadvantage of this parametric method is related to the not orthogonality. Hicks-Henne functions are not orthogonal which unable them from representing the complete set of continuous functions that vanish at the endpoints $x = 0$ and $x = 1$.

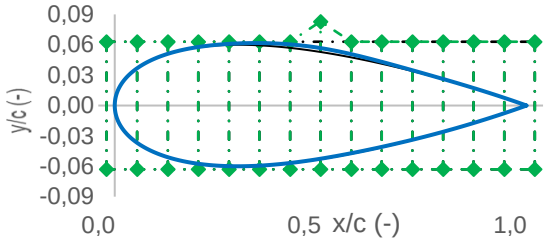

(a) Deformed and undeformed FFD box with 15 control points. Black lines indicate undeformed shape.

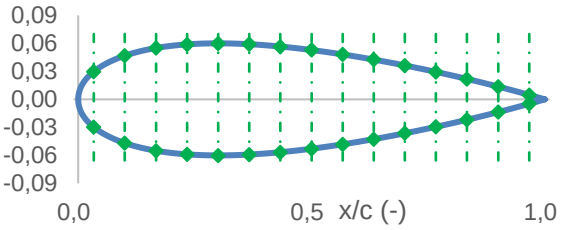

(b) Green points over the airfoils indicates bump maximum positions of 15 bumps.

Figure 1 - NACA 0012 airfoil embedded in an FFD box (a) and an even distribution of the Hicks-Henne method (b).

3. An open-source framework

In the current study, an open-source framework to perform ASO, resorting to three open-source software, is presented. As mesh generator SALOME software is used and for pre- and post-processing SU2 and ParaView will be considered, respectively. In addition, scripts in Python programming language were developed to link the different open-source software. As the first step, an initial baseline geometry is required to design the desirable starting airfoil. A python script was developed to enable the transformation of the airfoil coordinates into a format capable to be read by the mesh generator. The script was programmed such that for a given airfoil a design is generated. Once the mesh is generated around the airfoil all the information about the elements and points, together with the connectivities and boundaries, will be exported to a file in a native SU2 format. The mesh generator used does not allow for a direct exportation of the mesh into a SU2 native format. With a python script, which was programmed for that purpose, it had become possible to link this mesh generator with the SU2 solver. The mesh file is then taken as an input to the shape optimization cycle together with the selected objective function (I), constraints and a vector of design variables (D) (based on the selected parameterization method). A gradient-based optimizer using the adjoint method is then enabled to drive the design cycle, and the iterative design loop will proceed until one of the optimization convergence criterions is fulfilled. This ASO framework is illustrated in Figure 2. The most relevant modules from the SU2 code used for the design optimization in this work are: SU2_CFD (performs flow and adjoint analysis by solving governing PDEs); SU2_DEF (computes the geometry surface deformations and deforms the surrounding volume mesh given a set of design variables in the optimization process) and SU2_DOT (used for computing design gradients) [15]. When the gradient of the objective function (∇I) is computed, the gradient-based optimization algorithm is called to guide the search for the optimal solution.

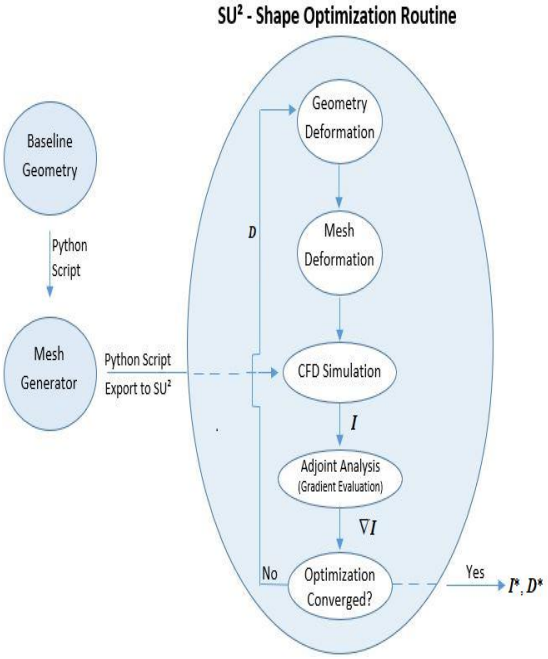

Figure 2 - Open-source framework: optimization procedure

4. Results

Two cases of study were employed to evaluate the impact of the selected parameterization methods. The first one consists in minimizing the drag coefficient of RAE 2822 airfoil, which is a test case of the AIAA Aerodynamic Design Optimization Discussion Group (ADODG). In the second case, the aim is to maximize the lift to drag ratio for two Mach conditions, starting from a NACA 0012 airfoil.

A. Case 1: Drag minimization of the RAE2822 airfoil

The drag minimization of the RAE 2822 airfoil in transonic viscous flow requires solving the RANS equations. A freestream Mach number of 0.734, an angle of attack of 2.79, a Reynolds number of 6.5 million, and a free-stream temperature of 288.15K are assumed for the optimization. The optimization problem can be formulated with its objective function and constraints as follows:

$$\begin{aligned} &\text{minimize} && C_d \\ &\text{subject to} && C_l = 0.824 \\ & && C_m \geq -0.092 \\ & && S_{airfoil} \geq \left(S_{airfoil}\right)_{baseline} \end{aligned}$$

A hybrid mesh with a C-topology is used considering a far-field boundary condition positioned approximately at 80 chord lengths, no-slip and adiabatic wall condition applied to the airfoil geometry. A mesh convergence study with three levels of refinement was performed. Relative errors between the medium and the fine grid of 0.92% and 1.43% for C_l and C_d, respectively, were obtained. The results obtained for the medium mesh were compared with the experimental ones with a C_d relative difference of 1.63%. All design optimizations were performed using the medium mesh. To examine the effect of design space dimensionality, the optimizations with the FFD control points and the Hicks-Henne approach were conducted varying the number of design variables from 6 to 30. The optimization results obtained with the FFD method are plotted in Figure 3, from which a similar behaviour is found between the considered sets of design variables. Starting in the leading edge until 40% of the chordwise, the curvature in upper surface of the baseline airfoil is reduced, which causes a flow deceleration and a smother pressure recovery hence eliminating the shock (as one can observe in Figure 3(b) from the pressure coefficient distribution). However, downstream the trailing edge, an increase of the airfoil thickness is achieved, satisfying the $S_{airfoil}$. Similar pattern exists for the surface perturbation as well as C_p distribution for all FFD cases. The constraints imposed were all respected resulting in an area increase of 0.4% regarding the airfoil baseline area.

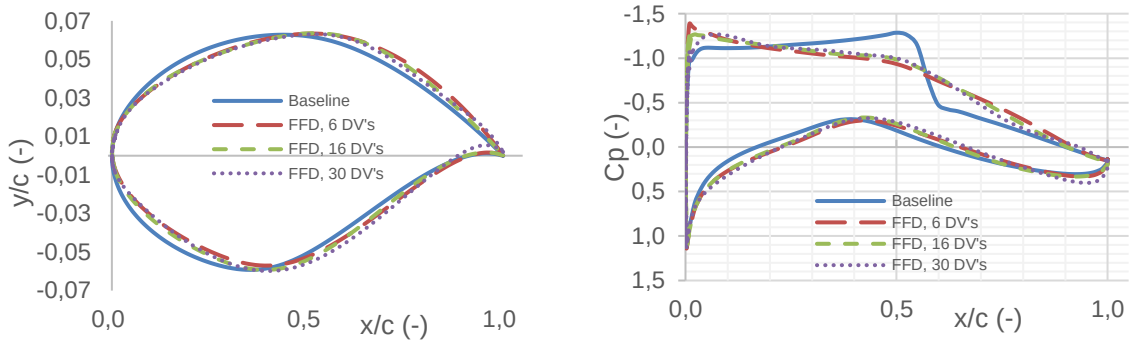

(a) **(b)**

Figure 3 - Case 1: Influence of design variables dimensionality on the optimization results using the FFD parameterization method: (a) Airfoil shapes and (b) pressure coefficient distribution.

The optimization results obtained for the Hicks-Henne parameterization method has not allowed to achieve feasible results for the drag reduction due to not respecting the constraints imposed. Both C_l and $\left(S_{airfoil}\right)_{baseline}$ are below the values imposed to the optimizer with a relative difference of 0.3% and 14.4%, respectively. Only the C_m is respected with a relative difference of approximately 6.3%. All optimizations were performed until they met one of the stop criteria imposed in the configuration file.

The results achieved are in good agreement with the ones obtained by other researchers with different parameterization techniques (see Table 1). From the comparison of the achieved values for the minimization of C_d, one can notice that the results of the present method are well within the bounds achieved by other researchers. Comparing the present result for the FFD approach with respect to the similar gradient-based approaches, both the performance and the computational effort (measured here in total number of functions evaluated) levels are in agreement.

Table 1 – Case 1: RAE 2822 optimization airfoil: comparison with other researchers results.

Reference Articles	Initial C_d	Optimized C_d	Reduction C_d (%)	Parameterization Method	Gradient-based Optimizer	DV Number	FE
Carrier et al. [32]	0.0202	0.0111	45.0	Bézier and B-Spline	SLSQP	10	25
Lee et al. [33]	0.0234	0.0132	43.6	B-Splines and FFD	SNOPT	34	250
Bisson et al. [34]	0.0178	0.01071	42.7	Third-order B-Spline	SNOPT	16	25
Yang and Ronch [35]	0.0241	0.01514	38.0	Hicks-Henne bump functions	SNOPT	30	-
Present	0.0196	0.01275	34.9	FFD	SLSQP	26	47

B. Case 2: Maximization of lift to drag ratio of NACA 0012

The maximization of the lift to drag ratio of a modified NACA 0012 airfoil, considering inviscid flow, for two free-stream Mach numbers is investigated to analyze the impact of the parametric methods on the initial geometry. The Mach numbers analyzed cover the transonic (0.85) and supersonic (2.0) regimes for an angle of attack fixed at 0º. The governing equation is the 2-D Euler equation with a free-stream temperature of 288.15K. A minimum thickness constraint greater than or equal to one percent of the chord along the entire chord length is imposed. The optimization problem can be summarized as:

$$\text{Maximize:} \quad {}^{L}/_{D}$$

$$\text{subject to:} \quad y \geq 0.01 \cdot \left(y_{(i)_{x/c}}\right), \mathrm{i} \in \left\{\frac{1}{4}, \frac{1}{3}, \frac{1}{2}, \frac{2}{3}, \frac{3}{4}\right\}, \forall\, x \in [0,1]$$

where x is the x-coordinate of a point on the airfoil, y is the y-coordinate of a point on the optimized airfoil, and $y(i)_{x/c}$ is the y-coordinate of the corresponding point on the airfoil where the thickness constrains are imposed. A modified NACA 0012 airfoil with zero-thickness trailing edge is defined following [36].

A structured C-topology grid around the NACA 0012 airfoil is generated. The far-field boundaries are placed at 50 chord lengths away from the airfoil surface. Far-field conditions are applied to the outer domain and the Euler wall boundary conditions to the airfoil. A grid convergence study with three meshes was performed to evaluate the evolution of the drag coefficient. The same mesh and correspondent mesh study was applied for both Mach numbers. Between the level of refinement of the medium and fine meshes, the resolution of 0.119 drag counts (1 drag count is equal to a C_d of $1 \cdot 10^{-4}$) is achieved for the transonic case and relative error less than 1% for the supersonic case. Despite the small penalty in the accuracy of the results, the medium mesh is chosen for all the analyses performed considering both flow conditions.

The parameters of the abovementioned methods, FFD and Hicks-Henne, were investigated for this case study. Firstly, for the FFD method, the box enclosing the airfoil was set such that it reduces its dimensions without intersecting the airfoil surface. Then the dimensional space was explored considering a varying number of control points which are the design variables set for the optimization considering this method. Secondly, for the Hicks-Henne method, two different set of parameters were evaluated: the width bump control parameter t_i; and the number of design variables.

Regarding the number of design variables, both FFD and Hicks-Henne methods presented similar behavior for the two Mach number considered. As the number of design variables increase, the lift to drag ratio also increase accompanied by an increase of the number of design cycles, which was found to be lower for the Hicks-Henne method. In what

concerns the width bump control parameter t_i of the Hicks-Hennes method, its increase has led to the reduction of the objective function (observed to be more effective in transonic conditions) since its increase allows for a more localized shape control (visible from the changes in the trailing edge region).

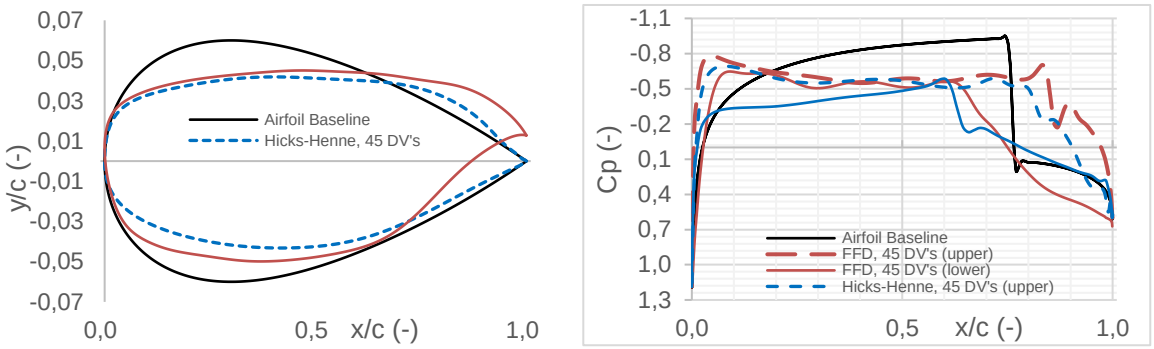

(a) **(b)**

Figure 4 - Case 2: Comparison of optimization results obtained from using the FFD control points and Hicks-Henn bump functions as parameterization methods: (a) airfoil shapes and (b) pressure coefficient distributions (M = 0.85, α = 0º and 45 DV's).

Herein, only the results for the maximum number of design variables considered (45) are discussed, similar behavior was observed for the others sets of design variables. Common to both flow regimes is the trend to modify the shape such that a pressure difference is generated (see Figure 4 Figure 5 (b)) to increase lift and an overall airfoil area is decreased (see Figure 4 Figure 5 (a)) to reduce drag, thus increasing lift to drag ratio. The formation of an incidence angle was found for the FFD method in both flow regimes, which was not possible to attain with the Hick-Henne method that has fix positions at the leading and trailing edges. Considering the transonic case, one may find resemblances with a supercritical airfoil (suitable for this flow regime) with the optimized shape considering the FFD method, which was not achieved with the Hicks-Henne method for the same reason as for the formation of the incidence angle. For the supersonic case, the shape considerable change to deflect the detached shock and increase lift to drag ratio by increase lift (a small increase in drag was in fact observed). The results are summarized in Table 2.

Table 2 - Lift to drag ratio results considering 45 design variables.

	Transonic	*Supersonic*
FFD method	228	1.18
Hicks-Henne method	251	0.69

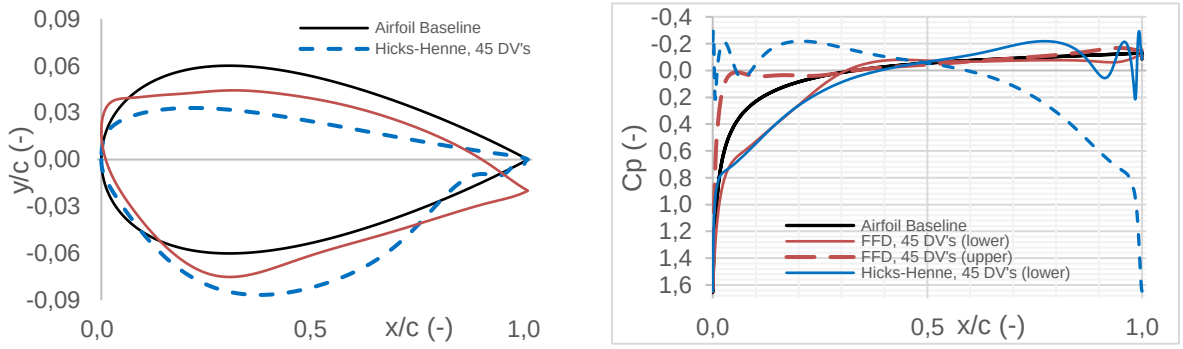

(a) **(b)**

Figure 5 - Case 2: Comparison of optimization results obtained from using the FFD control points and Hicks-Henn bump functions as parameterization methods: (a) airfoil shapes and (b) pressure coefficient distributions (M = 2.0, α = 0º and 45 DV's).

5. Conclusions

An aerodynamic optimization shape framework resorting to open source codes was implemented and applied to a benchmarking optimization case, achieving results in good agreement with those found in the literature. The implemented framework was then applied to a different case study to evaluate the effect that different parameters, of the selected parametrization methods, have on the aerodynamic shape optimization. This case study consists in

maximizing the lift to drag ratio of a NACA 0012 airfoil at zero degrees of angle of attack in transonic and supersonic conditions. Within the evaluated parameters, the increase of the number of design variables allowed for reaching higher lift to drag ratio at a higher computational cost, which was observed to be smaller using the Hicks-Henne method than the FFD method. In what concerns the Hicks-Henne method, the width bump control parameter was observed to provide more local control as it is increased. In overall, both methods were able to increase the lift to drag ratio by generating lift (through an increase of pressure difference between surfaces) and reducing area (which reduced the drag in transonic case and not in the supersonic case). In terms of the resulting transonic shapes, the FFD shape resembles a supercritical airfoil (suitable for this flow conditions) which was not possible with the Hicks-Henne since it is not possible to change the leading and trailing edge positions. For the supersonic conditions the shapes was such that they reduce the airfoil area and allow to deflect the detached shock and thus increase lift to drag ratio.

6. Reference

[1] J. R. R. A. Martins and J. T. Hwang, “Review and Unification of Methods for Computing Derivatives of Multidisciplinary Computational Models,” *AIAA J.*, vol. 51, no. 11, pp. 2582–2599, 2013.

[2] A. Jameson, “Aerodynamic design via control theory,” *J. Sci. Comput.*, vol. 3, no. 3, pp. 233–260, 1988.

[3] O. Baysal and M. E. Eleshaky, “Aerodynamic sensitivity analysis methods for the compressible {E}uler equations,” *J. Fluids Eng.*, vol. 113, no. 4, pp. 681–688, 1991.

[4] O. Baysal and M. E. Eleshaky, “Aerodynamic Design Optimization Using Sensitivity Analysis and Computational Fluid Dynamics,” *AIAA J.*, vol. 30, no. 3, pp. 718–725, 1992.

[5] W. K. Anderson and D. L. Bonhaus, “Airfoil Design on Unstructured Grids for Turbulent Flows,” *AIAA J.*, vol. 37(2), no. 2, pp. 185–191, 1999.

[6] S. K. Nadarajah, “Aerodynamic Design Optimization: Drag Minimization of the NACA 0012 in Transonic Inviscid Flow,” pp. 1–4, 2013.

[7] G. B. Cosentino and T. L. Holst, “Numerical optimization design of advanced transonic wing configurations[J],” *J. Aircr.*, vol. 23, no. 3, pp. 192–199, 1986.

[8] E. J. Nielsen and W. K. Anderson, “Aerodynamic Design Optimization on Unstructured Meshes Using the Navier-Stokes Equations,” *AIAA J.*, vol. 37, no. 11, pp. 1411–1419, 1999.

[9] Z. Lyu, G. K. W. Kenway, and J. R. R. A. Martins, “Aerodynamic Shape Optimization Investigations of the Common Research Model Wing Benchmark,” *AIAA J.*, vol. 53, no. 4, pp. 968–985, 2015.

[10] J. Reuther, A. Jameson, J. Farmer, L. Martinelli, and D. Saunders, “Aerodynamic shape optimization of complex aircraft configurations via an adjoint formulation,” *34th Aerosp. Sci. Meet. Exhib.*, no. January, 1996.

[11] W. K. Anderson and V. Venkatakrishnan, “Aerodynamic design optimization on unstructured grids with a continuous adjoint formulation,” *Comput. Fluids*, vol. 28, no. 4–5, pp. 443–480, 1999.

[12] J. Elliott and J. Peraire, “Aerodynamic optimization on unstructured meshes with viscous effects,” *AIAA Pap.*, vol. 97, p. 1849, 1997.

[13] A. Jameson, N. a. Pierce, and L. Martinelli, “Optimum aerodynamic design using the Navier-Stokes equations,” *35th Aerosp. Sci. Meet. Exhib. AIAA Pap. 97-0101*, no. January, 1997.

[14] C. Hirsch, *Numerical computation of internal and external flows, Volume 1: Fundamentals of Computational Fluid Dynamics*. 2007.

[15] T. D. Economon, F. Palacios, S. R. Copeland, T. W. Lukaczyk, and J. J. Alonso, “SU2: An Open-Source Suite for Multiphysics Simulation and Design,” *AIAA J.*, vol. 54, no. 3, pp. 1–19, 2015.

[16] F. Palacios *et al.*, “Stanford University Unstructured (SU 2): Open-source Analysis and Design Technology for Turbulent Flows,” no. January, pp. 1–33, 2014.

[17] C. Hirsch, *Numerical computation of internal and external flows, Volume 2: Computational Methods for inviscid and Viscous flows*. 2007.

[18] F. Palacios *et al.*, “Stanford University Unstructured (SU 2): An open-source integrated computational environment for multi-physics simulation and design .,” no. January, pp. 1–60, 2013.

[19] P. Hewitt, “Aerofoil Optimisation Using CST Parameterisation in SU2 Aerofoil Optimisation Using CST Parameterisation in,” no. August, 2014.

[20] R. M. Hicks, “Wing Design by Numerical Optimization,” vol. 15, no. 7, pp. 407–412, 1978.

[21] T. W. Sederberg and S. R. Parry, “Free-form deformation of solid geometric models,” *Proc. 13th Annu. Conf. Comput. Graph. Interact. Tech. - SIGGRAPH ’86*, vol. 20, no. 4, pp. 151–160, 1986.

[22] C. Lee, D. Koo, and D. W. Zingg, “Comparison of B-Spline Surface and Free-Form Deformation Geometry Control for Aerodynamic Optimization,” *AIAA J.*, vol. 55, no. 1, pp. 228–240, 2017.

[23] S. Coquillart, “Extended free-form deformation: a sculpturing tool for 3D geometric modeling,” *ACM SIGGRAPH Comput. Graph.*, vol. 24, no. 4, pp. 187–196, 1990.

[24] T. W. Sederberg, “Computer Aided Geometric Design - Course Notes,” 2011.

[25] E. I. Amoiralis and I. K. Nikolos, “Freeform Deformation Versus B-Spline Representation in Inverse Airfoil Design,” *J. Comput. Inf. Sci. Eng.*,

vol. 8, no. 2, p. 024001, 2008.

[26] S. S. Sarakinos, E. Amoiralis, and I. K. Nikolos, “Exploring Freeform Deformation Capabilities in Aerodynamic Shape Parameterization,” *EUROCON 2005 - Int. Conf. Comput. as a Tool""*, vol. 1, pp. 49–52, 2005.

[27] R. P. Liem, J. R. R. A. Martins, and G. K. W. Kenway, “Expected drag minimization for aerodynamic design optimization based on aircraft operational data,” *Aerosp. Sci. Technol.*, vol. 63, pp. 344–362, 2017.

[28] F. Of and M. Engineering, “Institute of Aerospace Engineering Adaptive Parameterization for Aerodynamic Shape Optimization in Aeronautical Applications,” 2015.

[29] V. Sripawadkul, M. Padulo, and M. Guenov, “A Comparison of Airfoil Shape Parameterization Techniques for Early Design Optimization,” *13th AIAA/ISSMO Multidiscip. Anal. Optim. Conf.*, no. September, pp. 1–9, 2010.

[30] A. Aerospace, S. Meeting, A. Aerospace, and S. Meeting, “Transonic Airfoil and Wing Design Using Inverse and Direct Methods,” 2015.

[31] D. A. Masters, N. J. Taylor, T. C. S. Rendall, C. B. Allen, and D. J. Poole, “Geometric Comparison of Aerofoil Shape Parameterization Methods,” *AIAA J.*, no. Article in Advance, pp. 1–15, 2017.

[32] G. Carrier *et al.*, “Gradient - Based Aerodynamic Optimization with the elsA Software,” *52nd Aerosp. Sci. Meet.*, no. January, pp. 1–31, 2014.

[33] C. Lee, D. Koo, K. Telidetzki, H. Buckley, H. Gagnon, and D. W. Zingg, “Aerodynamic Shape Optimization of Benchmark Problems Using Jetstream,” *53rd AIAA Aerosp. Sci. Meet.*, no. January, 2015.

[34] D. Shi-Dong, C.-H. Chen, and S. Nadarajah, “Adjoint-Based Aerodynamic Optimization of Benchmark Proble,” *35th AIAA Appl. Aerodyn. Conf.*, no. January, pp. 1–20, 2017.

[35] G. Yang and A. Da Ronch, “Aerodynamic Shape Optimisation of Benchmark Problems Using SU2,” *2018 AIAA/ASCE/AHS/ASC Struct. Struct. Dyn. Mater. Conf.*, no. January, pp. 1–28, 2018.

[36] Christopher Rumsey, “2D NACA 0012 Airfoil Validation.” [Online]. Available: https://turbmodels.larc.nasa.gov/naca0012_val.html. [Accessed: 22-Sep-2018].